



# Cooperative Guidance and Collision Avoidance for Multiple Pursuers

Bhargav Jha,\* Ronny Tsalik,<sup>†</sup> Martin Weiss,<sup>‡</sup> and Tal Shima<sup>§</sup>  
*Technion—Israel Institute of Technology, 3200003 Haifa, Israel*

DOI: 10.2514/1.G004139

**This paper presents a cooperative guidance law for an  $n$ -on- $n$  engagement scenario that ensures target interception and collision avoidance between the pursuers along with minimizing their team effort. The guidance law is derived using linear quadratic optimal control theory for a linearized engagement model. The pursuers cooperate with each other to accommodate differences in maneuver capabilities of different team members. A special case of 2-on-2 engagement is also analyzed, for which analytical closed-form formulas for the pursuer's guidance law are obtained. Various simulation results and experimental validation results, exemplifying the cooperation in different engagements, are also presented.**

## I. Introduction

**A**UTONOMOUS vehicles are capable of sensing their environment and traversing without a human operator. In recent times, they have become increasingly popular due to their wide applications in civilian as well as military domains. The automation of these vehicles has several components such as environment sensing and recognition, localization, and motion planning or control. The focus of this paper lies on the motion control aspect. This aspect aims at formulating a control strategy that steers a pursuer from an initial point to a target point. The pursuer can be an unmanned vehicle, a robot, or even a missile, whereas the target can be a waypoint, a landmark, or an adversary that has to be intercepted. In most real-world scenarios, the guidance of a pursuer to a given target point is coupled with the task of avoiding collisions with obstacles that can be stationary or moving.

Some of the current approaches for collision detection and avoidance are guidance-based, such as velocity obstacle method [1], collision cone approach [2,3], and the more recent avoidance mapping technique [4]. In [1], Fiorini and Shiller have proposed a collision avoidance method for circular-shaped obstacles moving at a constant speed. A set of velocities leading to collision is calculated for a given radius of the obstacle. To avoid the incoming obstacle, a command is generated based on actuator constraints such that the pursuer achieves a velocity that lies outside the set of collision velocities. In [2], Chakravarthy and Ghose have derived the collision conditions based on the components of the relative velocity along and perpendicular to the line of sight. The region of collision velocities can be avoided by applying maneuvers such as change of speed or lateral acceleration. Based on the collision cone approach, a proportional navigation (PN) based avoidance strategy is proposed in [3] by Han et al. Here, a relative velocity vector joining the pursuer and the safety boundary of the other pursuer in collision is selected, and PN guidance is used to steer the pursuer out of collision. A more recent approach based on avoidance map is proposed in [4] by Tony et al. The avoidance map is a mapping that indicates whether a particular maneuver can lead to a collision. It is represented in the plane of lateral accelerations of the two pursuers and is partitioned

into sectors involving collision and sectors not involving collision. Based on this information, a maneuver is selected to steer the pursuers out of collision.

The aforementioned collision avoidance strategies suffer from three major drawbacks.

1) They do not consider any kind of cooperation in scenarios with multiple pursuers, which may lead to significant deviation of the pursuers from the planned or nominal trajectory.

2) They are not optimal in terms of any of the parameters such as energy requirement, length of the path, or deviation from the nominal trajectory.

3) The collision avoidance is performed sequentially in two steps. The first step is collision detection, followed by a second step that generates collision avoidance maneuver. This leads to performance degradation.

The problem of sequential detection and avoidance can be overcome by an artificial potential field function. Here, the detection and avoidance step is integrated in one step. Classically, this kind of collision avoidance method was proposed in [5] for robotic manipulators. In [6], Rimon and Koditschek have extended this approach to the guidance of robots in the presence of obstacles. The disadvantage of this approach is the possibility of the pursuer getting trapped in local minima of the potential surface, and therefore it is unable to reach the target point in cases where the target and obstacles are placed close to each other. In [7], Ge and Cui have proposed a new repulsive potential function by taking the relative distance between the obstacle and the target point into consideration. This ensures that the target point is the global minimum of the total potential. Because the relation between the potential field function and the vehicle performance is not straightforward, it is difficult to optimize the performance of such collision avoidance methods.

In scenarios where pursuers work as a team, the collision avoidance strategies can be cooperative in nature. Based on the velocity obstacle approach, a cooperative collision avoidance strategy was developed in [8] by Snape et al., in which each pursuer shares equal responsibility for avoiding the impending collision. The control command is selected as close as possible to the current maneuver of each pursuer to ensure minimum deviation. In [9], Sunkara and Chakravarthy have proposed two kinds of cooperative avoidance strategies based on collision conditions mentioned in [2]. The first strategy involves acceleration magnitudes of the two pursuers as inputs, and the second involves the direction of acceleration vectors as inputs. Using dynamic inversion techniques, a control law was derived for pursuers to cooperatively drive each other out of the collision region.

In [10], Zapoteczny-Anderson and Ford have formulated collision avoidance for a single aircraft as an optimal control problem that ensures minimum deviation from the desired course while avoiding other aircraft. The system here is nonlinear, and hence numerical optimization techniques have been used to solve the problem. Menon and Park [11] provide a comprehensive review of collision avoidance

Received 12 October 2018; revision received 31 December 2018; accepted for publication 2 January 2019; published online 18 February 2019. Copyright © 2019 by the authors. Published by the American Institute of Aeronautics and Astronautics, Inc., with permission. All requests for copying and permission to reprint should be submitted to CCC at [www.copyright.com](http://www.copyright.com); employ the eISSN 1533-3884 to initiate your request. See also AIAA Rights and Permissions [www.aiaa.org/randp](http://www.aiaa.org/randp).

\*Ph.D. Student, Faculty of Aerospace Engineering; [jhabhargav@campus.technion.ac.il](mailto:jhabhargav@campus.technion.ac.il).

<sup>†</sup>Ph.D. Student, Faculty of Aerospace Engineering; [rtsalik@campus.technion.ac.il](mailto:rtsalik@campus.technion.ac.il).

<sup>‡</sup>Researcher, Faculty of Aerospace Engineering; [weissm@technion.ac.il](mailto:weissm@technion.ac.il).

<sup>§</sup>Professor, Faculty of Aerospace Engineering; [tal.shima@technion.ac.il](mailto:tal.shima@technion.ac.il).

approaches in case of multiple aircraft using optimal control theory. In [12], Menon et al. have developed collision avoidance algorithms based on the assumption that the nominal trajectories of the aircraft can be parameterized as a sequence of four-dimensional (three position coordinates and a time coordinate) waypoints. These waypoints are adjusted to generate optimal trajectories that satisfy the collision avoidance constraints and minimize desired cost functions. Škrjanc and Klančar have proposed an optimal cooperative collision avoidance strategy for multiple pursuers in [13]. In this work, a precomputed path for each pursuer is generated by minimizing the sum of the length of paths for all pursuers and taking into account the collision between them. To track these trajectories, a model predictive controller is designed. The offline generation of trajectory makes the implementation cumbersome and computationally expensive. The strategies proposed in [10,13] lack a closed-form expression for the guidance, making the analysis difficult. In [14], Weiss and Shima have proposed a closed-form solution of a guidance law for a pursuer to intercept a target while avoiding a static obstacle. Extending this approach, Kumar et al. have proposed a closed-form solution of a guidance law for a single pursuer to avoid multiple obstacles along with interception of a target at a certain impact angle in [15]. Both the proposed guidance laws in [14,15] minimize the control effort of the pursuer while minimizing the energy requirements. Along with this, the collision detection and avoidance occur simultaneously. However, as mentioned before, this guidance law is only for the case of a single pursuer and static obstacles.

In this paper, we develop a cooperative guidance law for multiple pursuers that steers them to their corresponding target points, along with achieving collision avoidance between them. The developed guidance law optimizes the total control effort of the team of pursuers with different penalties on the control effort for each member. This has two advantages. First, it reduces the fuel consumption of the pursuers. Second, this enables teaming of pursuers with different maneuver capabilities and therefore achieves our goals even when some of the pursuers are not as maneuverable as the other ones.

The paper is organized in the following way. In the next section, we describe the engagement scenario and obtain the nonlinear and linearized engagement kinematics. In Sec. III, the problem is formulated as an optimal control problem. Based on this formulation, a cooperative guidance law for  $n$  pursuers is derived in Sec. IV. A special case of two pursuers is analyzed in Sec. V, in which a closed-form optimal guidance law is presented. Results from simulations and experimental validation are presented in Sec. VI. This is followed by conclusions of the work in Sec. VII.

## II. Engagement Geometry

A planar engagement of  $n$  pursuers pursuing  $n$  targets is considered. Figure 1 shows the endgame engagement geometry in  $X - O - Y$  Cartesian inertial reference frame. Here,  $P_i$  and  $P_j$  denote the  $i$ th and  $j$ th pursuers. Similarly,  $T_i$  and  $T_j$  denote the targets. For

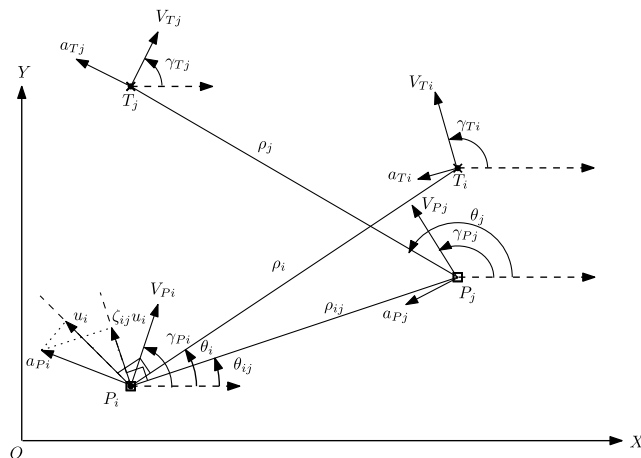


Fig. 1 Engagement geometry.

the sake of simplicity, we enumerate the target with the same index as that of its pursuer.  $V_{P_i}$  and  $V_{T_i}$  represent the velocity vectors of the  $i$ th pursuer and target, respectively. Their heading angles are denoted by  $\gamma_{P_i}$  and  $\gamma_{T_i}$ .  $\rho_i$  represents the range between the  $i$ th pursuer–target pair. Similarly, their relative line of sight (LOS) angle is denoted by  $\theta_i$ . The relative separation between the  $i$ th and  $j$ th pursuer is denoted as  $\rho_{ij}$ , and the LOS angle between them is denoted by  $\theta_{ij}$ .  $a_{P_i}$  denotes the acceleration of the pursuer, and  $a_{T_i}$  is the target acceleration. For any  $i$ th pursuer–target pair,  $u_i$  is the projection of pursuer’s acceleration  $a_{P_i}$  on the line perpendicular to the LOS joining the pursuer–target pair.  $\zeta_{ij}u_i$  is the component of acceleration  $a_{P_i}$  on the line perpendicular to the LOS joining the  $i$ th and  $j$ th pursuers.

For a collision to happen between a given pair of pursuers, it is assumed that the predicted point of collision between the pursuers is around the collision triangle formed between each pursuer and its respective target. In the case of  $n$  pursuers, the maximum number of possible collisions between any pair of pursuers is  $\binom{n}{2}$ . To reduce

computational needs, we may assume that there exists a higher-order collision detector that identifies pairs of pursuers that are “almost on the collision course” and therefore eliminates some of the collisions. In the absence of such collision detection mechanisms, we can assume all possible collisions between the pursuers. Now, we introduce some notations to denote the possible collisions. A collision between the  $i$ th and  $j$ th pursuers is expressed as a 2-tuple  $\{i, j\}$ , where  $i < j$ . Furthermore, all the possible collisions are arranged in an ascending order of the first pursuer index followed by the second pursuer index. This ordered set is denoted as  $\Omega$ . The  $k$ th element of the ordered set is denoted as  $\Omega_k$ , and the cardinality of the set ( $\Omega$ ) is denoted as  $K$ . The ordering of the set  $\Omega$  is done to make the definition of matrices concise in later sections. It is not necessarily related to the sequence in which the collisions take place.

Two collisions are called “related collisions” if they share a common pursuer. For a given collision  $\{i, j\}$ , another collision (say  $\{a, b\}$ ) is called “I-related” to  $\{i, j\}$  if the first pursuer  $i$  is involved in the collision (i.e., either  $a = i$  or  $b = i$ ). It is called “II-related” to  $\{i, j\}$ , if the second pursuer  $j$  is involved in the collision (i.e., either  $a = j$  or  $b = j$ ). For every collision  $\Omega_k$ , we denote the set of I-related collisions as  $S_{\Omega_k}^I$ . Similarly,  $S_{\Omega_k}^{II}$  denotes the set of II-related collisions for  $\Omega_k$ .

### A. Nonlinear Engagement Kinematics

The engagement kinematics of a pursuer–target pair is expressed in a polar coordinate system  $(\rho_i, \theta_i)$  attached to the  $i$ th pursuer and is expressed by the following equations:

$$\dot{\rho}_i = V_{T_i} \cos(\gamma_{T_i} - \theta_i) - V_{P_i} \cos(\gamma_{P_i} - \theta_i) \quad i \in \{1, \dots, n\} \quad (1)$$

$$\rho_i \dot{\theta}_i = V_{T_i} \sin(\gamma_{T_i} - \theta_i) - V_{P_i} \sin(\gamma_{P_i} - \theta_i) \quad i \in \{1, \dots, n\} \quad (2)$$

Without loss of generality, the engagement kinematics between the  $i$ th and  $j$ th pursuers is also defined in a polar coordinate system  $(\rho_{ij}, \theta_{ij})$ , which is attached to the  $i$ th pursuer, where  $i < j$ . It is expressed by the following set of equations:

$$\dot{\rho}_{ij} = V_{P_j} \cos(\gamma_{P_j} - \theta_{ij}) - V_{P_i} \cos(\gamma_{P_i} - \theta_{ij}) \quad \{i, j\} \in \Omega \quad (3)$$

$$\rho_{ij} \dot{\theta}_{ij} = V_{P_j} \sin(\gamma_{P_j} - \theta_{ij}) - V_{P_i} \sin(\gamma_{P_i} - \theta_{ij}) \quad \{i, j\} \in \Omega \quad (4)$$

During the endgame, the target and the pursuer are assumed to move at constant speeds. Therefore, once the collision triangle is achieved, the interception time to the targets ( $t_i^f$ ) can be expressed in terms of initial range  $\rho_i^0$  and closing speed of the pursuer–target pair ( $V_{c_i} \triangleq -\dot{\rho}_i$ ) as

$$t_i^f = \frac{\rho_i^0}{V_{c_i}} \quad i \in \{1, \dots, n\} \quad (5)$$

Similarly, when the  $i$ th and  $j$ th pursuers are on a collision course, the final time for collision ( $t_{ij}^f$ ) is expressed in terms of

initial range  $\rho_{ij}^0$  and the closing speed between  $i$ th and  $j$ th pursuers ( $V_{c_{ij}} \triangleq -\dot{\rho}_{ij}$ ) as

$$t_{ij}^f = \frac{\rho_{ij}^0}{V_{c_{ij}}}, \quad \{i, j\} \in \Omega \quad (6)$$

The dynamics of the acceleration of all the pursuers and the targets are assumed to be ideal. Therefore, the changes in heading angles ( $\gamma_{Pi}, \gamma_{Ti}$ ) due to accelerations of the pursuer ( $a_{Pi}$ ) and the target ( $a_{Ti}$ ) appear as

$$\dot{\gamma}_{Pi} = \frac{a_{Pi}}{V_{Pi}} \quad i \in \{1, \dots, n\} \quad (7)$$

$$\dot{\gamma}_{Ti} = \frac{a_{Ti}}{V_{Ti}} \quad i \in \{1, \dots, n\} \quad (8)$$

## B. Linearized Engagement Kinematics

It is assumed that the deviations of the pursuers and the targets from their respective collision triangles are small. Therefore, a linearization of the engagement kinematics around the collision triangles is obtained. Based on this linearized model, a guidance law for capturing the target while avoiding collision between the pursuers is derived thereafter.

The relative displacement normal to the LOS between the  $i$ th pursuer and its corresponding target is denoted as  $y_i$ . Similarly,  $y_{ij}$  denotes the relative displacement normal to the LOS between the  $i$ th and  $j$ th pursuers. The state vector of the entire engagement can then be expressed as

$$\mathbf{x} = \left[ y_{I_1} \quad \dot{y}_{I_1} \quad \dots \quad y_{I_n} \quad \dot{y}_{I_n} \quad y_{C_1} \quad \dot{y}_{C_1} \quad \dots \quad y_{C_K} \quad \dot{y}_{C_K} \right]^T \quad (9)$$

where  $y_I \in \mathbb{R}^n$  and  $y_C \in \mathbb{R}^K$  are the vectors comprising the displacements perpendicular to the line of sights for interceptions and collisions, respectively. They are defined as follows:

$$y_{Ii} = y_i \quad i \in \{1, \dots, n\} \quad (10)$$

$$y_{Ck} = y_{ij}, \text{ where } \{i, j\} = \Omega_k \quad k \in \{1, \dots, K\} \quad (11)$$

The linearized equations of motion are obtained as follows:

$$\dot{x}_{2m-1} = x_{2m} \quad m \in \{1, \dots, n\} \quad (12)$$

$$\dot{x}_{2m} = a_{Tm}^n - u_m, \quad m \in \{1, \dots, n\} \quad (13)$$

$$\dot{x}_{2k+1} = x_{2k+2} \quad k \in \{n, \dots, n+K\} \quad (14)$$

$$\dot{x}_{2k+2} = \zeta_{ji} u_j - \zeta_{ij} u_i, \quad k \in \{n, \dots, n+K\} \text{ and } \{i, j\} = \Omega_k \quad (15)$$

Here,  $x_i, i \in \{1, \dots, 2(n+K)\}$  represents  $i$ th coordinate of the state vector  $\mathbf{x}$ , and  $K$  denotes the cardinality of set  $\Omega$ . The displacement between a given pair of pursuers is affected by the component of their accelerations that is normal to the LOS joining them. Therefore, in Eq. (15), the terms  $\zeta_{ij}$  and  $\zeta_{ji}$  are introduced as shown in Fig. 1. The target and pursuers remain close to the collision course, and in such scenarios, it can be assumed that  $\zeta_{ij}$  and  $\zeta_{ji}$  are dependent only on the initial values of the LOS angles ( $\theta_i^0, \theta_j^0, \theta_{ij}^0$ ) and the initial heading angles of the pursuers ( $\gamma_{Pi}^0, \gamma_{Pj}^0$ ). For each pair  $\{i, j\} \in \Omega$ , the expressions of  $\zeta_{ij}$  and  $\zeta_{ji}$  are

$$\zeta_{ij} = \frac{\cos(\gamma_{Pi}^0 - \theta_{ij}^0)}{\cos(\gamma_{Pi}^0 - \theta_i^0)} \quad (16)$$

$$\zeta_{ji} = \frac{\cos(\gamma_{Pj}^0 - \theta_{ij}^0)}{\cos(\gamma_{Pj}^0 - \theta_j^0)} \quad (17)$$

$a_{Ti}^n$  and  $u_i$  are the components of the accelerations normal to LOS between the  $i$ th pursuer–target pair for the target and pursuer, respectively. Hence, the relation between these components of acceleration and the acceleration of the  $i$ th target and  $i$ th pursuer pair is given by

$$a_{Ti}^n = a_{Ti} \cos(\gamma_{Ti}^0 - \theta_i^0) \quad i \in \{1, \dots, n\} \quad (18)$$

$$u_i = a_{Pi} \cos(\gamma_{Pi}^0 - \theta_i^0) \quad i \in \{1, \dots, n\} \quad (19)$$

Using Eqs. (12–19), the linearized system of equations can also be written in the form of matrices as

$$\dot{\mathbf{x}} = \mathbf{A}\mathbf{x} + \mathbf{B}\mathbf{u} + \mathbf{C}\mathbf{v} \quad (20)$$

where  $\mathbf{u} = [u_1 \quad \dots \quad u_n]^T$  and  $\mathbf{v} = [a_{T1}^n \quad \dots \quad a_{Tn}^n]^T$ . The matrices  $\mathbf{A}$ ,  $\mathbf{B}$ , and  $\mathbf{C}$  are given by

$$\mathbf{A} = \mathbf{I}_{2(n+K)} \otimes \mathbf{A}_I, \quad \mathbf{B} = \begin{bmatrix} \mathbf{I}_n \otimes \mathbf{B}_I \\ [\mathbf{B}_c]_{K \times n} \end{bmatrix}, \quad \mathbf{C} = \begin{bmatrix} \mathbf{I}_n \otimes \mathbf{C}_I \\ [\mathbf{0}]_{K \times n} \end{bmatrix} \quad (21)$$

where  $\otimes$  denotes the Kronecker product of two matrices,  $\mathbf{I}_n \in \mathbb{R}^n$  is an identity matrix, and  $[\mathbf{0}] \in \mathbb{R}^{K \times n}$  is a zero matrix. The matrices  $\mathbf{A}_I$ ,  $\mathbf{B}_I$ , and  $\mathbf{C}_I$  are given as

$$\mathbf{A}_I = \begin{bmatrix} 0 & 1 \\ 0 & 0 \end{bmatrix}, \quad \mathbf{B}_I = \begin{bmatrix} 0 \\ -1 \end{bmatrix}, \quad \mathbf{C}_I = \begin{bmatrix} 0 \\ 1 \end{bmatrix} \quad (22)$$

The matrix  $\mathbf{B}_c \in \mathbb{R}^{K \times n}$  is obtained as

$$\mathbf{B}_{ckj} = \begin{cases} -\zeta_{jx}, & \text{if } \Omega_k = \{j, x\} \\ \zeta_{jx}, & \text{if } \Omega_k = \{x, j\}, \quad x \in \{1, \dots, n\} \\ 0, & \text{otherwise} \end{cases} \quad (23)$$

## III. Optimization Problem Formulation

The goal here is to derive a minimum effort guidance law for a team of  $n$  pursuers intercepting  $n$  maneuvering targets while avoiding collision between themselves. To achieve this, the relative distance between the  $i$ th pursuer–target pairs ( $y_i$ ) should be zero at the intercept time  $t_i^f$ . Along with this, the relative distance between any  $i$ th and  $j$ th pursuers should be greater than a safe limit  $R_{ij}$  at the predicted time of collision  $t_{ij}^f$ . We impose these constraints as hard constraints in the problem formulation and express them as follows:

$$y_i(t_i^f) = 0 \quad i \in \{1, \dots, n\} \quad (24)$$

$$y_{ij}(t_{ij}^f) \geq R_{ij} \quad \{i, j\} \in \Omega \quad (25)$$

For minimizing the total control effort of the team of pursuers, the cost function is defined as

$$J = \sum_{i=1}^n \frac{\alpha_i}{2} \int_{t_0}^{t_i^f} u_i^2 dt \quad (26)$$

where  $\alpha_0$  is the penalty on the control effort of the  $i$ th pursuer. The lower the maneuvering capability of the  $i$ th pursuer is, the higher the corresponding weight  $\alpha_i$  should be.

### A. Order Reduction Using Zero-Effort-Miss Transformation

The order of system (20) can be reduced from  $2(n+K)$  to  $(n+K)$  using the zero-effort-miss transformation [16]. Another

advantage of using this transformation is that the transformed states become a function of the control inputs only, and therefore it simplifies the calculation of Lagrange multipliers, as we will see in the next section. The transformation of the variables associated with the  $i$ th pursuer is given by [17]

$$z_i(t) = \mathbf{D}\Phi(t_i^f, t)\mathbf{x}(t) + \mathbf{D} \int_t^{t_i^f} \Phi(t_i^f, \tau)\mathbf{C}\mathbf{v} d\tau \quad i \in \{1, \dots, n\} \quad (27)$$

where  $\Phi(t_i^f, t)$  is the transition matrix associated with matrix  $\mathbf{A}$  in Eq. (20),  $z_i$  is the zero-effort-miss distance between the  $i$ th pursuer–target pair, and  $\mathbf{D} \in \mathbb{R}^{(n+K)}$  is a constant row vector that selects the appropriate element of the state vector. For example, to obtain the zero-effort-miss for the  $i$ th pursuer–target pair, the vector  $\mathbf{D}$  is defined as

$$\mathbf{D}_k = \begin{cases} 1, & \text{if } k = i \\ 0, & \text{otherwise} \end{cases} \quad (28)$$

At any given instance, the ZEM distance for a pursuer–target pair is defined as the distance by which a pursuer will miss the target, if the pursuer applies no further acceleration and the target performs the expected maneuver. Using the preceding transformation, the expression for ZEM distance ( $z_i$ ) is obtained, under the assumption of a constant target maneuver, as

$$z_i(t) = y_i(t) + \dot{y}_i(t_i^f - t) + \frac{a_{Ti}^n(t_i^f - t)^2}{2} \quad (29)$$

Similarly, for the pursuer–pursuer pair, the ZEM distance ( $z_{ij}$ ) is defined as the achieved separation distance between them at the time of closest approach, if both of them apply no further acceleration. Using the ZEM transformation as before, the ZEM distances between two pursuers can be expressed as

$$z_{ij}(t) = y_{ij}(t) + \dot{y}_{ij}(t_{ij}^f - t) \quad (30)$$

The evolution of these ZEM distances with time can be expressed by the following state equations:

$$\dot{z}_i(t) = -(t_i^f - t)u_i \mathbb{1}(t_i^f) \quad i \in \{1, \dots, n\} \quad (31)$$

$$\dot{z}_{ij}(t) = -(t_{ij}^f - t)(\zeta_{ij}u_i - \zeta_{ji}u_j) \mathbb{1}(t_{ij}^f) \quad \{i, j\} \in \Omega \quad (32)$$

Here, the step function is defined as

$$\mathbb{1}(\tau) = \begin{cases} 1 & t < \tau \\ 0 & t \geq \tau \end{cases}$$

It should be noted that the ZEM distance is not defined once the pursuer reaches the target and achieves its objective. Also, the ZEM distance for a pursuer–pursuer pair also remains the same as  $z_{ij}(t_{ij}^f)$ , beyond the time of closest approach. Therefore, we have introduced a unit step function  $\mathbb{1}(\tau)$  in the transformed state equations in Eqs. (31) and (32). The transformed state equations can also be expressed in matrix form as follows:

$$\dot{\mathbf{z}} = \mathbf{B}_z \mathbf{u} \quad (33)$$

Here,

$$\mathbf{z} = [\mathbf{z}_I \quad \mathbf{z}_C]^T \quad \text{and} \quad \mathbf{z}_I = [z_1 \quad \dots \quad z_n]^T, \quad \mathbf{z}_C = z_{ij},$$

where  $\{i, j\} = \Omega_k \quad k \in \{1, \dots, K\}$  (34)

The matrix  $\mathbf{B}_z \in \mathbb{R}^{(n+K) \times n}$  is defined as

$$\mathbf{B}_z = \begin{bmatrix} [\mathbf{B}_z I]_{n \times n} \\ [\mathbf{B}_z C]_{K \times n} \end{bmatrix}$$

where

$$\mathbf{B}_{zIij} = \begin{cases} -(t_i^f - t)\mathbb{1}(t_i^f), & \text{if } i = j \\ 0, & \text{otherwise} \end{cases}$$

$$\mathbf{B}_{zCkj} = \begin{cases} -\zeta_{jx}(t_{jx}^f - t)\mathbb{1}(t_{jx}^f), & \text{if } \Omega_k = \{j, x\} \\ \zeta_{jx}(t_{xj}^f - t)\mathbb{1}(t_{xj}^f), & \text{if } \Omega_k = \{x, j\}, \quad x \in \{1, \dots, n\} \\ 0, & \text{otherwise} \end{cases} \quad (35)$$

From Eqs. (29) and (30) and the constraints mentioned in Eqs. (24) and (25), we obtain the constraints for the transformed states as

$$N_i(z_i(t_i^f), t_i^f) \triangleq z_i(t_i^f) = 0, \quad i \in \{1, \dots, n\} \quad (36)$$

$$N_{ij}(z_{ij}(t_{ij}^f), t_{ij}^f) \triangleq z_{ij}(t_{ij}^f) - z_{ij}^d = 0, \quad \{i, j\} \in \Omega \quad (37)$$

where  $z_{ij}^d$  is an arbitrary variable whose absolute value is greater than the safe distance ( $|z_{ij}^d| \geq R_{ij}$ ). The final time for the entire engagement is defined as the time when the last interception takes place. Thus, we define the final time of the entire engagement as  $t^f = \max(t_1^f, \dots, t_n^f)$ . Also, we can assume that  $t_{ij}^f \leq \min(t_i^f, t_j^f)$ , which signifies that the possible collision between a pair of pursuers takes place before or at the time when any one of the pursuers intercepts its corresponding target. Because of these assumptions, in Eqs. (36) and (37), the constraint corresponding to the last interception is the terminal constraint of our problem. Other constraints that occur before the final interception are the interior point constraints.

## B. Reduced Order Optimal Control Problem

Using the transformed states and constraints, the optimal control problem is formulated as

$$\dot{z}_i(t) = -(t_i^f - t)u_i \mathbb{1}(t_i^f) \quad N_i(z_i(t_i^f), t_i^f) = 0 \quad i \in \{1, \dots, n\} \quad (38)$$

$$\dot{z}_{ij}(t) = -(t_{ij}^f - t)(\zeta_{ij}u_i - \zeta_{ji}u_j) \mathbb{1}(t_{ij}^f) \quad N_{ij}(z_{ij}(t_{ij}^f), t_{ij}^f) = 0 \quad \{i, j\} \in \Omega \quad (39)$$

The cost function in Eq. (26) can be rewritten as the sum of the control effort of each pursuer over the entire engagement as

$$J = \frac{1}{2} \int_{t_0}^{t^f} \mathbf{u}^T \mathbf{P} \mathbf{u} dt = \sum_{i=1}^n \frac{\alpha_i}{2} \int_{t_0}^{t^f} u_i^2 dt \quad (40)$$

where  $\mathbf{P}$  is a positive-definite weight matrix defined as

$$\mathbf{P}_{ij} = \begin{cases} \alpha_i, & \text{if } i = j \\ 0, & \text{otherwise} \end{cases}$$

## IV. Guidance Law Derivation

In the previous section, the problem was formulated as a linear quadratic optimal control problem in which a set of terminal and interior point constraints have to be satisfied and the state equations are discontinuous at those interior points. The solution of this class of problems is discussed in detail in [16,18]. We will use the necessary conditions for optimality mentioned in [16] to derive the guidance law.

The Hamiltonian  $\mathcal{H}$  of the optimization problem formulated in Sec. III.A can be written as

$$\begin{aligned} \mathcal{H} &= \frac{1}{2} \mathbf{u}^T \mathbf{P} \mathbf{u} + \lambda^T \mathbf{B}_z \mathbf{u} \\ &= \sum_{i=1}^n \left( \frac{\alpha_i u_i^2}{2} - \lambda_i (t_i^f - t) u_i \mathbb{1}(t_i^f) \right) \\ &\quad - \sum_{\{i,j\} \in \Omega} \lambda_{ij} (t_{ij}^f - t) (\zeta_{ij} u_i - \zeta_{ji} u_j) \mathbb{1}(t_{ij}^f) \end{aligned} \quad (41)$$

where  $\lambda_i$ ,  $i \in \{1, \dots, n\}$  is the Lagrange multiplier associated with the states corresponding to the  $i$ th target interception, and  $\lambda_{ij}$ ,  $\{i, j\} \in \Omega$  is the Lagrange multiplier associated with the states corresponding to the collision between the  $i$ th and  $j$ th pursuers. The Lagrange multiplier vector  $\lambda$  is defined as

$$\begin{aligned} \lambda &= [\lambda_I \ \lambda_C]^T \\ \lambda_I &= [\lambda_1 \ \dots \ \lambda_n]^T, \quad \lambda_C = \lambda_{ij}, \quad \text{where } \{i, j\} \in \Omega_k \quad k \in \{1, \dots, K\} \end{aligned} \quad (42)$$

*Proposition 1:* In the proposed linear quadratic optimal control formulation with interior and terminal point constraints, where the cost function and the dynamics of the transformed system are independent of the state variables, the control input of each pursuer is a piecewise linear function of time.

*Proof:* The Lagrange multipliers must satisfy the following condition along the optimal trajectory:

$$\dot{\lambda} = -\mathcal{H}_z \quad (43)$$

The dynamics of the transformed system [Eqs. (38) and (39)] are independent of the state variables; therefore, we have

$$\dot{\lambda} = 0 \quad (44)$$

In addition to the condition mentioned in Eq. (43), at the time of each target interception ( $t_i^f$ ), the Lagrange multipliers  $\lambda_i$  should satisfy the following necessary conditions (Sec. 3.7 in [16]):

$$\lambda_i(t_i^f+) = \frac{\partial J}{\partial z_i} \quad i \in \{1, \dots, n\} \quad (45)$$

$$\lambda_i(t_i^f-) = \lambda_i(t_i^f+) + \nu_i \frac{\partial N_i}{\partial z_i} \Big|_{t=t_i} \quad i \in \{1, \dots, n\} \quad (46)$$

where  $\nu_i$  is a nonzero coefficient, and  $(t_i^f-)$  and  $(t_i^f+)$  signify time just before and after  $t_i^f$ , respectively. Obtaining the derivative of the constraints and the cost function with respect to  $z_i$ , we get

$$\frac{\partial J}{\partial z_i} = 0, \quad \frac{\partial N_i}{\partial z_i} \Big|_{t=t_i} = 1 \quad i \in \{1 \dots n\} \quad (47)$$

From Eqs. (45–47), we have

$$\lambda_i(t_i^f-) = \nu_i, \quad \lambda_i(t_i^f+) = 0 \quad i \in \{1, \dots, n\} \quad (48)$$

Similar conditions as in Eqs. (45–47) will also hold at the interior point constraints corresponding to all the times of collisions ( $t_{ij}^f$ ). Thus, we have

$$\lambda_{ij}(t_{ij}^f-) = \nu_{ij}, \quad \lambda_{ij}(t_{ij}^f+) = 0 \quad \{i, j\} \in \Omega \quad (49)$$

where  $\nu_{ij}$  is a nonzero coefficient, and  $(t_{ij}^f-)$  and  $(t_{ij}^f+)$  signify time just before and after  $t_{ij}^f$ , respectively. From Eqs. (44), (48), and (49), we conclude that the Lagrange multipliers are piecewise constants.

Along the optimal trajectory, the Hamiltonian is minimized by the control input. Therefore, we have the following condition:

$$\mathcal{H}_u = 0 \quad (50)$$

From this condition, we obtain the control inputs as

$$\mathbf{u} = -\mathbf{P}^{-1} \mathbf{B}_z^T \lambda$$

that is,

$$\begin{aligned} u_i &= \frac{1}{\alpha_i} \left( \lambda_i (t_i^f - t) \mathbb{1}(t_i^f) - \sum_{\substack{j=1 \\ \{i,j\} \in \Omega}}^{i-1} \lambda_{ji} (t_{ji}^f - t) \zeta_{ij} \mathbb{1}(t_{ji}^f) \right. \\ &\quad \left. + \sum_{\substack{j=i+1 \\ \{i,j\} \in \Omega}}^n \lambda_{ij} (t_{ij}^f - t) \zeta_{ij} \mathbb{1}(t_{ij}^f) \right), \quad i \in \{1, \dots, n\} \end{aligned} \quad (51)$$

Because the Lagrange multipliers are piecewise constant with discontinuities at the interior points [Eqs. (48) and (49)], from Eq. (51) we conclude that the control input for each pursuer will be a piecewise linear function of time.  $\square$

The  $(n + K)$  constants for the value of Lagrange multipliers [Eqs. (48) and (49)] can be obtained by satisfying the constraints on ZEM distances as defined in Eqs. (31) and (32). Integrating these equations, we get

$$\int_{t_0}^{t_i^f} (t_i^f - t) u_i dt = z_i(t_0) \quad i \in \{1, \dots, n\} \quad (52)$$

$$\int_{t_0}^{t_{ij}^f} (t_{ij}^f - t) (\zeta_{ij} u_i - \zeta_{ji} u_j) dt = z_{ij}(t_0) - z_{ij}^d \quad \{i, j\} \in \Omega \quad (53)$$

The difference between the final interception (or predicted collision) time and the current time is expressed as the time-to-go parameters. They are defined as

$$t_i^g \triangleq t_i^f - t, \quad t_{ij}^g \triangleq t_{ij}^f - t \quad (54)$$

The variables  $t_i^g$  and  $t_{ij}^g$  are the time-to-go for the interception of target and time-to-go for collision of the pursuers, respectively. For each pair of pursuers  $(i, j)$  heading toward possible collision ( $\{i, j\} \in \Omega$ ), the difference between the time of interception of their targets ( $t_i^f$ ,  $t_j^f$ ) and their corresponding time of collision ( $t_{ij}^f$ ) is denoted as

$$\Delta_{ij} \triangleq t_i^f - t_{ij}^f \quad (55)$$

$$\Delta_{ji} \triangleq t_j^f - t_{ij}^f \quad (56)$$

Substituting the preceding variables in Eqs. (52) and (53) and integrating them after plugging the value of control inputs from Eq. (51), we obtain the following:

$$\begin{aligned} \frac{\lambda_i (t_i^g)^3}{\alpha_i 3} + \sum_{\substack{j=i+1 \\ \{i,j\} \in \Omega}}^n \frac{\lambda_{ij} \zeta_{ij} (t_{ij}^g)^2}{\alpha_i 6} (\Delta_{ij} + 2t_i^g) \\ - \sum_{\substack{j=1 \\ \{i,j\} \in \Omega}}^{i-1} \frac{\lambda_{ji} \zeta_{ij} (t_{ij}^g)^2}{\alpha_i 6} (\Delta_{ij} + 2t_i^g) = z_i(t_0) \end{aligned} \quad (57)$$

$$\begin{aligned}
 & \lambda_{ij} \left( \frac{\zeta_{ij}^2}{\alpha_i} + \frac{\zeta_{ji}^2}{\alpha_j} \right) \frac{(t_{ij}^g)^3}{3} + \frac{\lambda_{ij} \zeta_{ij} (t_{ij}^g)^2}{\alpha_i} (\Delta_{ij} + 2t_i^g) \\
 & - \frac{\lambda_j \zeta_{ji} (t_{ij}^g)^2}{\alpha_j} (\Delta_{ji} + 2t_j^g) - \sum_{\substack{p=1 \\ \{p,j\} \in S_{\Omega_k}^-}}^{i-1} \frac{\lambda_{pj}}{6\alpha_i} \zeta_{ij} \zeta_{ip} (t_{pi}^g)^2 (3t_{ij}^g - t_{pi}^g) \\
 & - \sum_{\substack{p=1 \\ \{p,i\} \in S_{\Omega_k}^+}}^{i-1} \frac{\lambda_{pi}}{6\alpha_i} \zeta_{ij} \zeta_{ip} (t_{ij}^g)^2 (3t_{pi}^g - t_{ij}^g) + \sum_{\substack{p=i+1 \\ \{p,i\} \in S_{\Omega_k}^-}}^n \frac{\lambda_{ip}}{6\alpha_i} \zeta_{ij} \zeta_{ip} (t_{ip}^g)^2 (3t_{ij}^g - t_{ip}^g) \\
 & + \sum_{\substack{p=i+1 \\ \{p,i\} \in S_{\Omega_k}^+}}^n \frac{\lambda_{ip}}{6\alpha_i} \zeta_{ij} \zeta_{ip} (t_{ij}^g)^2 (3t_{ip}^g - t_{ij}^g) + \sum_{\substack{p=1 \\ \{p,j\} \in S_{\Omega_k}^-}}^{j-1} \frac{\lambda_{pj}}{6\alpha_j} \zeta_{ji} \zeta_{jp} (t_{pj}^g)^2 (3t_{ij}^g - t_{pj}^g) \\
 & + \sum_{\substack{p=1 \\ \{p,j\} \in S_{\Omega_k}^+}}^{j-1} \frac{\lambda_{jp}}{6\alpha_j} \zeta_{ji} \zeta_{jp} (t_{ij}^g)^2 (3t_{pj}^g - t_{ij}^g) - \sum_{\substack{p=j+1 \\ \{p,j\} \in S_{\Omega_k}^-}}^n \frac{\lambda_{jp}}{6\alpha_i} \zeta_{ji} \zeta_{jp} (t_{jp}^g)^2 (3t_{ij}^g - t_{jp}^g) \\
 & - \sum_{\substack{p=j+1 \\ \{p,j\} \in S_{\Omega_k}^+}}^n \frac{\lambda_{jp}}{6\alpha_j} \zeta_{ji} \zeta_{jp} (t_{ij}^g)^2 (3t_{jp}^g - t_{ij}^g) = z_{ij}(t_0) - z_{ij}^d \\
 & \{i, j\} \in \Omega
 \end{aligned} \tag{58}$$

where  $\Omega_k = \{i, j\}$ . The sets  $S_{\Omega_k}^+$  and  $S_{\Omega_k}^-$  are the sets of related collisions that take place before and after the collision  $\{i, j\}$ , respectively. They are defined as follows:

$$S_{\Omega_k}^+ = \{a, b\} \in S_{\Omega_k}^I \cup S_{\Omega_k}^{II} | t_{a,b}^f > t_{i,j}^f \} \tag{59}$$

$$S_{\Omega_k}^- = \{a, b\} \in S_{\Omega_k}^I \cup S_{\Omega_k}^{II} | t_{a,b}^f < t_{i,j}^f \} \tag{60}$$

Expressing Eqs. (57) and (58) as a system of linear equations in matrix form, we obtain

$$G \begin{bmatrix} \lambda_I \\ \lambda_C \end{bmatrix} = \begin{bmatrix} z_I \\ z_C - z_C^d \end{bmatrix}, \quad \text{where } G \triangleq \begin{bmatrix} G_I & G_{IC} \\ G_{IC}^T & G_C \end{bmatrix} \tag{61}$$

$\lambda_I, \lambda_C, z_I,$  and  $z_C$  are defined as in Eqs. (34) and (42), and

$$z_{Ck}^d \triangleq z_{ij}^d, \quad \text{where } \{i, j\} = \Omega_k \quad k \in \{1, \dots, K\} \tag{62}$$

The vector  $z_C^d \in \mathbb{R}^K$  is composed of the desired miss distances to be achieved between each pair of pursuers at their corresponding times of collision. The matrix  $G \in \mathbb{R}^{(n+K) \times (n+K)}$  is the system matrix for the linear system of equations in Eqs. (57) and (58). This matrix is expressed as a partition of four block matrices in Eq. (61). Among these block matrices, the matrix  $G_I \in \mathbb{R}^{n \times n}$  and  $G_C \in \mathbb{R}^{K \times K}$  are the matrices associated with terms involving interception and collision, respectively. They are defined as follows:

$$G_{Ikl} = \begin{cases} \frac{(t_k^g)^3}{3\alpha_k}, & \text{if } k = l \\ 0, & \text{otherwise} \end{cases} \tag{63}$$

For any two collisions  $\Omega_k = \{i, j\}$  and  $\Omega_l = \{a, b\}$ , the matrix  $G_C$  is defined as

$$G_{Ckl} = \begin{cases} \left( \frac{\zeta_{ij}^2}{\alpha_i} + \frac{\zeta_{ji}^2}{\alpha_j} \right) \frac{(t_{ij}^g)^3}{3}, & \text{if } k = l \\ -\frac{\zeta_{ij}}{6\alpha_i} \zeta_{ba} (t_{ab}^g)^2 (3t_{ij}^g - t_{ab}^g), & \text{if } k < l \text{ and } \Omega_l \in S_{\Omega_k}^- \cap S_{\Omega_k}^I \\ -\frac{\zeta_{ji}}{6\alpha_j} \zeta_{ba} (t_{ab}^g)^2 (3t_{ab}^g - t_{ij}^g), & \text{if } k < l \text{ and } \Omega_l \in S_{\Omega_k}^+ \cap S_{\Omega_k}^I \\ \frac{\zeta_{ij}}{6\alpha_i} \zeta_{ab} (t_{ab}^g)^2 (3t_{ij}^g - t_{ab}^g), & \text{if } k > l \text{ and } \Omega_l \in S_{\Omega_k}^- \cap S_{\Omega_k}^I \\ \frac{\zeta_{ji}}{6\alpha_j} \zeta_{ab} (t_{ab}^g)^2 (3t_{ab}^g - t_{ij}^g), & \text{if } k > l \text{ and } \Omega_l \in S_{\Omega_k}^+ \cap S_{\Omega_k}^I \\ \frac{\zeta_{ij}}{6\alpha_i} \zeta_{ba} (t_{ij}^g)^2 (3t_{ab}^g - t_{ij}^g), & \text{if } k < l \text{ and } \Omega_l \in S_{\Omega_k}^- \cap S_{\Omega_k}^{II} \\ \frac{\zeta_{ji}}{6\alpha_j} \zeta_{ba} (t_{ij}^g)^2 (3t_{ab}^g - t_{ij}^g), & \text{if } k < l \text{ and } \Omega_l \in S_{\Omega_k}^+ \cap S_{\Omega_k}^{II} \\ -\frac{\zeta_{ij}}{6\alpha_i} \zeta_{ab} (t_{ij}^g)^2 (3t_{ab}^g - t_{ij}^g), & \text{if } k > l \text{ and } \Omega_l \in S_{\Omega_k}^- \cap S_{\Omega_k}^{II} \\ -\frac{\zeta_{ji}}{6\alpha_j} \zeta_{ab} (t_{ij}^g)^2 (3t_{ab}^g - t_{ij}^g), & \text{if } k > l \text{ and } \Omega_l \in S_{\Omega_k}^+ \cap S_{\Omega_k}^{II} \\ 0, & \text{otherwise} \end{cases} \tag{64}$$

The matrix  $G_{IC} \in (n \times K)$  is given by

$$G_{ICkl} = \begin{cases} \frac{\zeta_{kx}}{6\alpha_k} (t_{kx}^g)^2 (\Delta_{kx} + 2t_k^g), & \text{if } \Omega_l = kx \\ -\frac{\zeta_{kx}}{6\alpha_k} (t_{kx}^g)^2 (\Delta_{kx} + 2t_k^g), & \text{if } \Omega_l = xk, \quad x \in \{1, \dots, n\} \\ 0, & \text{otherwise} \end{cases} \tag{65}$$

From Eq. (61) the Lagrange multipliers  $\lambda_I$  and  $\lambda_C$  can be obtained as

$$\begin{bmatrix} \lambda_I \\ \lambda_C \end{bmatrix} = G^{-1} \begin{bmatrix} z_I \\ z_C - z_C^d \end{bmatrix}, \quad \text{where } G^{-1} \triangleq \begin{bmatrix} G_{I1} & G_{I2} \\ G_{I2}^T & G_{I3} \end{bmatrix} \tag{66}$$

The matrix  $G$  is symmetric. Therefore,  $G^{-1}$  is also symmetric. The blocks of matrix  $G^{-1}$  can be computed in terms of the blocks of matrix  $G$  by the following expression [19]:

$$\begin{aligned}
 & \begin{bmatrix} G_{I1} & G_{I2} \\ G_{I2}^T & G_{I3} \end{bmatrix} \\
 & = \begin{bmatrix} (G_I - G_{IC} G_C^{-1} G_{IC}^T)^{-1} & -G_I^{-1} G_{IC} (G_C - G_{IC}^T G_I^{-1} G_{IC})^{-1} \\ -(G_C - G_{IC}^T G_I^{-1} G_{IC})^{-1} G_{IC}^T G_C^{-1} & (G_C - G_{IC}^T G_I^{-1} G_{IC})^{-1} \end{bmatrix}
 \end{aligned} \tag{67}$$

The matrix  $G^{-1}$  exists, provided that  $G_I^{-1}, G_C^{-1}, (G_C - G_{IC}^T G_I^{-1} G_{IC})^{-1}$  and  $(G_I - G_{IC} G_C^{-1} G_{IC}^T)^{-1}$  exist.

The total team effort can be expressed as follows by substituting the value of control inputs from Eq. (51) in the cost function:

$$\sum_{i=1}^n \int_{t_0}^{t_i} \frac{\alpha_i}{2} u_i^2 dt = \begin{bmatrix} z_I \\ z_C - z_C^d \end{bmatrix}^T \begin{bmatrix} G_{I1} & G_{I2} \\ G_{I2}^T & G_{I3} \end{bmatrix} \begin{bmatrix} z_I \\ z_C - z_C^d \end{bmatrix} \tag{68}$$

$$\begin{aligned}
 & = z_I^T G_{I1} z_I + (z_C - z_C^d)^T G_{I2} z_I + z_I^T G_{I2} (z_C - z_C^d) \\
 & \quad + (z_C - z_C^d)^T G_{I3} (z_C - z_C^d)
 \end{aligned} \tag{69}$$

$$\begin{aligned}
 & = \begin{bmatrix} z_I^T G_{I1} z_I + z_C^T G_{I2}^T z_I + z_I^T G_{I2} z_C + z_C^T G_{I3} z_C \\ - (G_{I3} z_C + G_{I2}^T z_I) G_{I3}^{-1} (G_{I3} z_C + G_{I2}^T z_I)^T \\ + \left[ (z_C^d - z_C - G_{I3}^{-1} G_{I2}^T z_I) G_{I3} (z_C^d - z_C - G_{I3}^{-1} G_{I2}^T z_I) \right] \end{bmatrix}
 \end{aligned} \tag{70}$$

The value of  $\mathbf{z}_C^d \in \mathbb{R}^K$  was considered to be arbitrary while formulating the optimal control problem [Eq. (37)]. Hence, to find the minimum of the total team effort, the desired zero-effort-miss distances corresponding to the collision are determined under the constraints of collision avoidance for each pair; that is  $|z_{ij}^d| \geq R_{ij}$ ,  $\{i, j\} \in \Omega$ . From Eq. (70), it can be noticed that the cost function is quadratic in  $\mathbf{z}_C^d$ . Therefore, the total control effort can be minimized by choosing appropriate value of  $\mathbf{z}_C^d$ . The minimum total control effort can be attained at the optimal value  $\mathbf{z}_C^{d*}$ , which is given by

$$\mathbf{z}_C^{d*} = \arg \min_{\mathbf{z}_C^d \in S} \left( \mathbf{z}_C^d - \mathbf{z}_C - G_{I3}^{-1} G_{I2}^T \mathbf{z}_I \right)^T G_{I3} \left( \mathbf{z}_C^d - \mathbf{z}_C - G_{I3}^{-1} G_{I2}^T \mathbf{z}_I \right) \quad (71)$$

where

$$S = \left\{ \mathbf{z}_C^d \in \mathbb{R}^K \mid |z_{ij}^d| \geq R_{ij}, \{i, j\} \in \Omega \right\} \quad (72)$$

Let us define

$$\mathbf{z}_{\text{col}} \triangleq \mathbf{z}_C + G_{I3}^{-1} G_{I2}^T \mathbf{z}_I \quad (73)$$

and let  $\Psi_{S, G_{I3}}(\cdot)$  be the generalized dead-zone function [15,20] associated with  $G_{I3}$  and the set  $S$  (see Appendix A for the general definition). Its value at  $\mathbf{z}_{\text{col}}$  is

$$\Psi_{S, G_{I3}}(\mathbf{z}_{\text{col}}) = G_{I3} \left( \mathbf{z}_C^{d*} - \mathbf{z}_{\text{col}} \right) \quad (74)$$

The following proposition expresses the optimal guidance command from Eq. (51) in terms of the value of the generalized dead-zone function at  $\mathbf{z}_{\text{col}}$ .

*Proposition 2:* The optimal guidance command is

$$\mathbf{u} = -\mathbf{P}^{-1} \left( \mathbf{B}_{zI}^T G_I^{-1} \mathbf{z}_I + \left( \mathbf{B}_{zI}^T G_I^{-1} G_{IC} - \mathbf{B}_{zC}^T \right) \Psi_{S, G_{I3}}(\mathbf{z}_{\text{col}}) \right)$$

*Proof:* In the rest of the text, for the sake of brevity, we denote  $\Psi_c = \Psi_{S, G_{I3}}(\mathbf{z}_{\text{col}})$ . From Eq. (74), we have

$$\mathbf{z}_C^{d*} = G_{I3}^{-1} \Psi_c + \mathbf{z}_{\text{col}} \quad (75)$$

Doing some algebraic manipulation, we obtain

$$\mathbf{z}_C - \mathbf{z}_C^{d*} = \mathbf{z}_C - G_{I3}^{-1} \Psi_c - \mathbf{z}_{\text{col}} = -G_{I3}^{-1} \Psi_c - G_{I3}^{-1} G_{I2}^T \mathbf{z}_I \quad (76)$$

Substituting this value into Eq. (66) and using Eq. (67) to express the blocks of  $G^{-1}$  in terms of the blocks of the matrix  $G$ , the value of Lagrange multipliers is obtained as

$$\begin{aligned} \begin{bmatrix} \lambda_I \\ \lambda_C \end{bmatrix} &= \begin{bmatrix} G_{i1} \mathbf{z}_I - G_{i2} G_{I3}^{-1} (\Psi_c + G_{I2}^T \mathbf{z}_I) \\ -\Psi_c \end{bmatrix} \\ &= \begin{bmatrix} G_I^{-1} (\mathbf{z}_I + G_{IC} \Psi_c) \\ -\Psi_c \end{bmatrix} \end{aligned} \quad (77)$$

Substituting the values of the Lagrange multiplier in Eq. (51), we obtain the control input vector as

$$\begin{aligned} \mathbf{u} &= -\mathbf{P}^{-1} \begin{bmatrix} \mathbf{B}_{zI}^T & \mathbf{B}_{zC}^T \end{bmatrix} \begin{bmatrix} \lambda_I \\ \lambda_C \end{bmatrix} \\ &= -\mathbf{P}^{-1} \left( \mathbf{B}_{zI}^T G_I^{-1} (\mathbf{z}_I + G_{IC} \Psi_c) - \mathbf{B}_{zC}^T \Psi_c \right) \\ &= -\mathbf{P}^{-1} \left( \mathbf{B}_{zI}^T G_I^{-1} \mathbf{z}_I + \left( \mathbf{B}_{zI}^T G_I^{-1} G_{IC} - \mathbf{B}_{zC}^T \right) \Psi_c \right) \end{aligned} \quad (78)$$

This completes the proof.  $\square$

The matrix  $G_I$  is a diagonal matrix, and therefore its inverse can be calculated by taking the reciprocal of the diagonal terms. Hence,  $G_I^{-1}$  is obtained as the following:

$$G_I^{-1} = \begin{cases} \frac{3\alpha_i}{(t_i^g)^3}, & \text{if } i = j \\ 0, & \text{otherwise} \end{cases} \quad (79)$$

We denote  $\Psi_k$  as the  $k$ th element of the vector  $\Psi_c$ . If a collision  $\{a, b\}$  is the  $k$ th element of the ordered set  $\Omega$ , we denote  $\Psi_{ab} \triangleq \Psi_k$ . Using this notation and Eq. (79), we simplify the optimal command obtained in Eq. (78) and express it for each pursuer as

$$\begin{aligned} u_i &= \frac{3z_i}{(t_i^g)^2} + \sum_{\substack{j=1 \\ \{i,j\} \in \Omega}}^{i-1} \frac{\zeta_{ij} t_{ij}^g \Delta_{ij} (t_i^g + \Delta_{ij}) \Psi_{ji}}{2\alpha_i (t_i^g)^2} \\ &\quad - \sum_{\substack{j=i+1 \\ \{i,j\} \in \Omega}}^n \frac{\zeta_{ij} t_{ij}^g \Delta_{ij} (t_i^g + \Delta_{ij}) \Psi_{ij}}{2\alpha_i (t_i^g)^2} \end{aligned} \quad (80)$$

The proposed guidance law requires the estimate of zero-effort-miss distances and time-to-go between various entities of the engagement scenario. The time-to-go information can be approximated using range information as shown in Eqs. (5), (6), and (54). The ZEM distances can be obtained by the following approximate relations:

$$z_i \approx (t_i^g)^2 V_{C_i} \dot{\theta}_i + \frac{1}{2} a_{T_i}^n (t_i^g)^2 \quad (81)$$

$$z_{ij} \approx (t_{ij}^g)^2 V_{C_{ij}} \dot{\theta}_{ij} \quad (82)$$

*Remark 1:* The proposed guidance law can be seen as augmented proportional navigation (APN) guidance with a bias term. The first term in Eq. (80) corresponds to APN guidance, and the rest of the terms correspond to the collision avoidance maneuver. Therefore, when the pursuer is not required to perform the collision avoidance maneuvers, the guidance law degenerates to APN.

## V. Case of Two Pursuers

In this section, we will investigate a special case of two pursuers and provide a closed-form analytical solution of the proposed guidance law.

### A. Analytic Solution of Guidance Law

In this case, there are two pursuers heading for interception of two targets while avoiding collision between them. Both the pursuers have similar maneuvering capabilities. Hence, the weights on their individual control effort are comparable. From Eqs. (63–65), the matrix  $G \in \mathbb{R}^{3 \times 3}$  for this case is given by

$$G = \begin{bmatrix} \frac{t_1^g}{\alpha_1} & 0 & \frac{\zeta_{12} t_{12}^g}{6\alpha_1} (\Delta_{12} + 2t_1^g) \\ 0 & \frac{t_2^g}{\alpha_2} & -\frac{\zeta_{21} t_{12}^g}{6\alpha_2} (\Delta_{21} + 2t_2^g) \\ \frac{\zeta_{12} t_{12}^g}{6\alpha_1} (\Delta_{12} + 2t_1^g) & -\frac{\zeta_{21} t_{12}^g}{6\alpha_2} (\Delta_{21} + 2t_2^g) & \left( \frac{\zeta_{12}^2}{\alpha_1} + \frac{\zeta_{21}^2}{\alpha_2} \right) \frac{t_{12}^g}{3} \end{bmatrix} \quad (83)$$

Using Eqs. (67) and (73), we obtain

$$\mathbf{z}_{\text{col}} = \mathbf{z}_C + G_{I3}^{-1} G_{I2}^T \mathbf{z}_I = \mathbf{z}_C - G_{IC}^T G_I^{-1} \mathbf{z}_I \quad (84)$$

Incorporating the values of  $G_{IC}$  and  $G_I^{-1}$  from Eqs. (65) and (79), we have

$$\begin{aligned}
z_{\text{col}} &= z_{12} - \left[ \frac{\zeta_{12} t_{12}^2}{6\alpha_1} (\Delta_{12} + 2t_1^g) - \frac{-\zeta_{21} t_{12}^2}{6\alpha_2} (\Delta_{21} + 2t_2^g) \right] \\
&\quad \times \begin{bmatrix} \frac{3\alpha_1}{t_1^3} & 0 \\ 0 & \frac{3\alpha_2}{t_2^3} \end{bmatrix} \begin{bmatrix} z_1 \\ z_2 \end{bmatrix} \\
&= z_{12} - \frac{\zeta_{12} t_{12}^2 (\Delta_{12} + 2t_1^g) z_1}{2t_1^3} + \frac{\zeta_{21} t_{12}^2 (\Delta_{21} + 2t_2^g) z_2}{2t_2^3}
\end{aligned} \quad (85)$$

In this case,  $z_{\text{col}}$  is a scalar because there is only one possible collision. From Eq. (67), the matrix  $G_{i3} \in \mathbb{R}^{1 \times 1}$  is obtained as

$$\begin{aligned}
G_{i3} &= \left[ \left( \frac{\zeta_{12}^2}{\alpha_1} + \frac{\zeta_{21}^2}{\alpha_2} \right) \frac{(t_{12}^g)^3}{3} - \frac{3\alpha_1}{(t_1^g)^3} \left( \frac{\zeta_{12}}{6\alpha_1} (t_{12}^g)^2 (\Delta_{12} + 2t_1^g) \right)^2 \right. \\
&\quad \left. - \frac{3\alpha_2}{(t_2^g)^3} \left( \frac{\zeta_{21}}{6\alpha_2} (t_{12}^g)^2 (\Delta_{21} + 2t_2^g) \right)^2 \right]^{-1} \\
&= \frac{12\alpha_1 \alpha_2 (t_1^g)^3 (t_2^g)^3}{\alpha_2 (t_2^g)^3 \zeta_{12}^2 (t_{12}^g)^3 \Delta_{12}^2 (3t_1^g + \Delta_{12}) + \alpha_1 (t_1^g)^3 \zeta_{21}^2 (t_{12}^g)^3 \Delta_{21}^2 (3t_2^g + \Delta_{21})}
\end{aligned} \quad (87)$$

Here, the dead-zone function  $\Psi_{S, G_{i3}}(\cdot): \mathbb{R}^1 \rightarrow \mathbb{R}^1$  is one-dimensional and is associated with the set

$$S = \left\{ z_{12}^d \in \mathbb{R} \mid |z_{12}^d| > R \right\} \quad (89)$$

where  $R$  is the desired safe distance between the two pursuers, and  $z_{12}^d$  is defined as in Eq. (32). The optimal value  $z_{12}^{d*}$  is obtained from Eq. (71) as

$$z_{12}^{d*} = \arg \min_{z_{12}^d \in S} (z_{12}^d - z_{\text{col}})^2 G_{i3} \quad (90)$$

Therefore,

$$z_{12}^{d*} = \begin{cases} z_{12}^d & |z_{12}^d| \geq R \\ R \operatorname{sign}(z_{12}^d) & |z_{12}^d| < R \end{cases} \quad (91)$$

From Eqs. (74) and (91), the dead-zone function can be expressed as

$$\Psi_{S, G_{i3}}(z_{\text{col}}) = G_{i3} (z_{12}^{d*} - z_{\text{col}}) = -G_{i3} \Psi_R(z_{\text{col}}) \quad (92)$$

where the function  $\Psi_R(x)$  is given as

$$\Psi_R(x) = \begin{cases} 0, & |x| > R \\ x - R, & 0 < x \leq R \\ x + R, & -R < x \leq 0 \end{cases} \quad (93)$$

Using the derived dead-zone function and Eq. (80), the guidance law for both the pursuers is given as

$$\begin{aligned}
u_1 &= \frac{3z_1}{(t_1^g)^2} \\
&\quad - \frac{6\alpha_2 t_1^g \zeta_{12} t_{12}^g \Delta_{12} (t_1^g + \Delta_{12}) (t_2^g)^3 \Psi_R(z_{\text{col}})}{\alpha_2 (t_2^g)^3 \zeta_{12}^2 (t_{12}^g)^3 \Delta_{12}^2 (3t_1^g + \Delta_{12}) + \alpha_1 (t_1^g)^3 \zeta_{21}^2 (t_{12}^g)^3 \Delta_{21}^2 (3t_2^g + \Delta_{21})}
\end{aligned} \quad (94)$$

$$\begin{aligned}
u_2 &= \frac{3z_2}{(t_2^g)^2} \\
&\quad + \frac{6\alpha_1 t_2^g \zeta_{21} t_{12}^g \Delta_{21} (t_2^g + \Delta_{21}) (t_1^g)^3 \Psi_R(z_{\text{col}})}{\alpha_2 (t_2^g)^3 \zeta_{12}^2 (t_{12}^g)^3 \Delta_{12}^2 (3t_1^g + \Delta_{12}) + \alpha_1 (t_1^g)^3 \zeta_{21}^2 (t_{12}^g)^3 \Delta_{21}^2 (3t_2^g + \Delta_{21})}
\end{aligned} \quad (95)$$

## B. Case of One Pursuer with Severely Limited Maneuver Capability

Now, we present the guidance law for the case, where one of the pursuers (say, second pursuer) has a severely limited maneuver capability. Thus, the penalty on the control effort for this pursuer can be set to a very large value ( $\alpha_2 \rightarrow \infty$ ). Equations (94) and (95) then reduce to the following:

$$\lim_{\alpha_2 \rightarrow 0} u_1 = \frac{3z_1}{(t_1^g)^2} - \frac{6t_1^g (t_1^g + \Delta_{12}) \Psi_R(z_{\text{col}})}{\zeta_{12} (t_{12}^g)^2 \Delta_{12} (3t_1^g + \Delta_{12})} \quad (96)$$

$$\lim_{\alpha_2 \rightarrow 0} u_2 = \frac{3z_2}{(t_2^g)^2} \quad (97)$$

From the preceding control inputs, it can be seen that the second pursuer does APN with a gain of 3, whereas the first pursuer performs APN along with the collision avoidance maneuver.

## VI. Simulations and Experimental Validation

In this section, we will present the results for simulations and experimental validation that were conducted to investigate the performance of the proposed guidance law for the case of two pursuers. Before the commencement of the engagement, we assume that the pursuer–target pairing has already been carried out based on various factors that can include distances to the targets, functional capabilities of the pursuers, etc. Once the engagement begins, the pursuers are locked on to their respective targets. For all the cases, the  $P_1 - T_1$  and  $P_2 - T_2$  pursuer–target pairing is assumed.

### A. Simulation Results

In all the simulations, the speeds of the pursuers ( $P_1, P_2$ ) and the targets ( $T_1, T_2$ ) are assumed to be constant. The minimum safe distance between the pursuers is  $R = 300$  m.

#### 1. Linear Simulations

Here, we present the simulation results of the linearized engagement kinematics, given by Eqs. (12–15), for the case of stationary targets. All the initial separations perpendicular to the corresponding line of sights are zero and the final times are  $t_1^f = 10.2$  s,  $t_2^f = 10.1$  s,  $t_3^f = 3.8$  s.

Figure 2 shows the cooperative collision avoidance between the pursuers where both the pursuers have the same penalty on their control effort  $\alpha_1 = 1$  and  $\alpha_2 = 1$ . From Fig. 2a, it can be seen that both the pursuers cooperate equally and avoid collision by achieving the safe separation of 300 m at the time of collision (3.8 s). Along with this, their separation from their corresponding targets goes to zero at their respective interception times. In Fig. 2b, the acceleration profile for the pursuer is linear, as can be justified from Proposition 1. A switch in acceleration occurs at the time of collision, after which both the pursuers perform APN for intercepting the target.

Figure 3 shows the case when one of the pursuers has severely limited acceleration capability. In this case, we choose a very high penalty on the control effort for this pursuer ( $\alpha_2 = 1000$ ). Because of this, only the first pursuer maneuvers to avoid collision between them, whereas the second pursuer only performs APN to reach its corresponding target. It can be seen from Fig. 3a that they successfully avoid collision by achieving the safe separation of 300 m at time of collision (3.8 s). In addition to this, the miss distance for each pursuer at the time of its respective interception is also zero. The acceleration profile in Fig. 3b shows that there is only one switch for

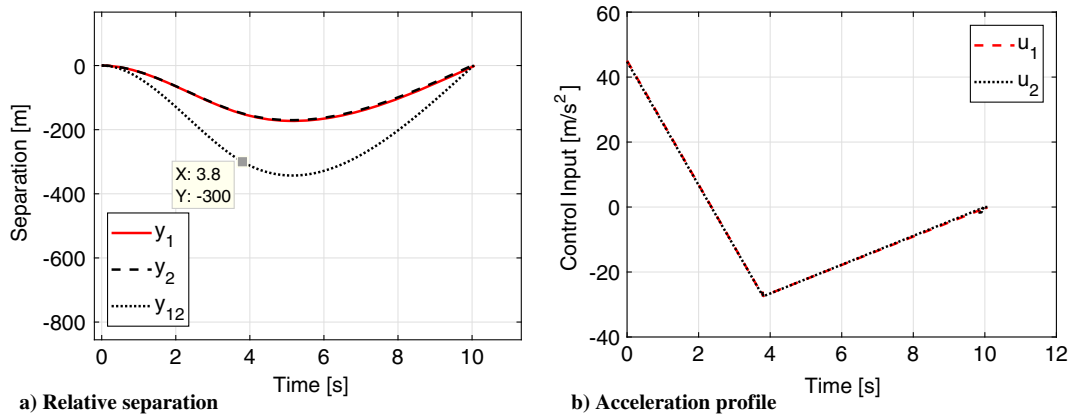


Fig. 2 Collision avoidance when the pursuers cooperate symmetrically ( $\alpha_1, \alpha_2 = 1$ ).

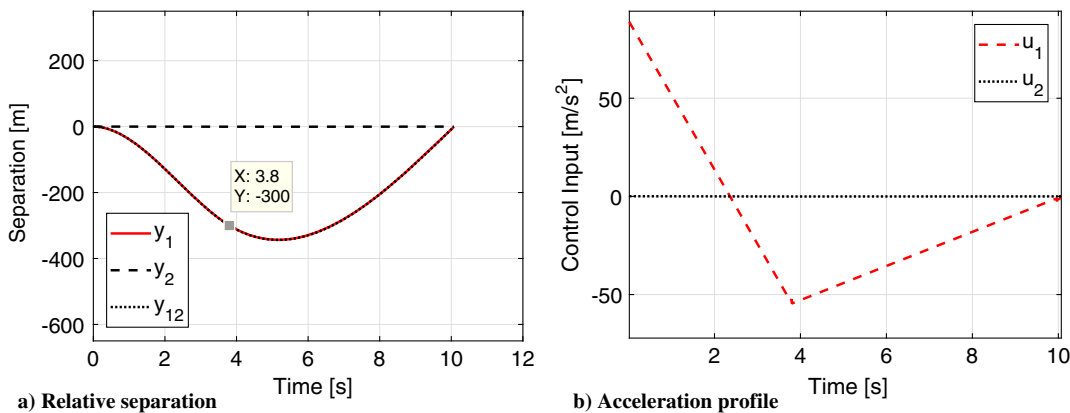


Fig. 3 Collision avoidance when one of the pursuers has a limited maneuver capability ( $\alpha_1 = 1, \alpha_2 = 1000$ ).

the second pursuer, whereas there is no switch in the acceleration profile for the first pursuer.

## 2. Nonlinear Simulations

The guidance law was derived assuming a linearized engagement model. Therefore, to evaluate the applicability of guidance law in nonlinear engagement scenario, we performed the simulation using nonlinear state equations as described in Sec. II.A. This section presents the performance of the guidance law in nonlinear engagement scenarios for both stationary targets (scenario 1) and targets maneuvering (scenario 2) with constant acceleration. The parameters for the simulation are summarized in Table 1.

Figure 4a shows the trajectories for the case when the targets are stationary and the pursuers have identical maneuver capabilities. The dotted line shows the initial LOS between each pursuer–target pair. Because both pursuers are cooperating equally, both deviate symmetrically from the initial LOS to avoid collision. The acceleration profile for each pursuer is also symmetric, as can be seen in Fig. 4c. For the same engagement scenario, Fig. 5a shows the case when the pursuers have different maneuvering capability. Here,

the second pursuer has 10 times higher penalty on the control effort than the first pursuer. Because of this, it can be noticed that the second pursuer deviates less than the first pursuer. Also, the acceleration requirement from the second pursuer is much less than that from the first pursuer (see Fig. 5c).

In Fig. 6, the second pursuer has severely limited maneuver capability, and therefore the penalty on its control effort is very high. The trajectories in Fig. 6a show that only the first pursuer deviates from the collision course to avoid collision. In the addition to this, from Fig. 6c it can be noticed that the second pursuer maneuvers negligibly. In all these cases, it can be seen from Figs. 4b, 5b, and 6b that the relative separation between the targets is more than the desired safe limit. Also, the similarity of the acceleration profiles in the nonlinear case (Figs. 4c, 5c, and 6c) to that of the linear case (Figs. 2b and 3b) backs the fact that the near-collision course approximations are valid during the entire engagement.

Now, we will present the case of constantly maneuvering targets. Figure 7a shows an engagement scenario in which the pursuers do not avoid each other while intercepting their corresponding targets. As shown in this figure, the pursuers collide with each other and therefore do not intercept the target. Figure 7b shows the trajectories of the pursuers when they use the proposed guidance laws to avoid collision and intercept the maneuvering targets. The relative separation achieved in this case is 386 m, which is more than the safe limit.

Table 1 Nonlinear simulation parameters

Parameter	Value (scenario 1)	Value (scenario 2)
Initial position of $P_1$ , m	(0, 0)	(0, 0)
Initial position of $P_2$ , m	(0, 5000)	(0, 5000)
Initial position of $T_1$ , m	(5000, 5000)	(0, 7000)
Initial position of $T_2$ , m	(0, 5000)	(0, -2000)
Speed of pursuers ( $V_{P_1}, V_{P_2}$ ), m/s	(700, 700)	(700, 700)
Speed of targets ( $V_{T_1}, V_{T_2}$ ), m/s	(0, 0)	(100, 100)
Target accelerations ( $a_{T_1}^x, a_{T_2}^y$ ), m/s <sup>2</sup>	(0, 0)	(-10, 10)
Minimum safe distance $R$ , m	300	300

## B. Experimental Validation

We conducted experimental validation of the proposed guidance law to test its applicability in a small indoor environment. The experiments were conducted in the Cooperative Autonomous Systems (CASYS) Laboratory at Technion, which serves as a testbed for research in cooperative guidance and control of aerial and ground vehicles. The description of the testbed is presented in Ref. [21]. The ground area for the experiment was  $3 \times 3$  m, and two Kobuki robotic

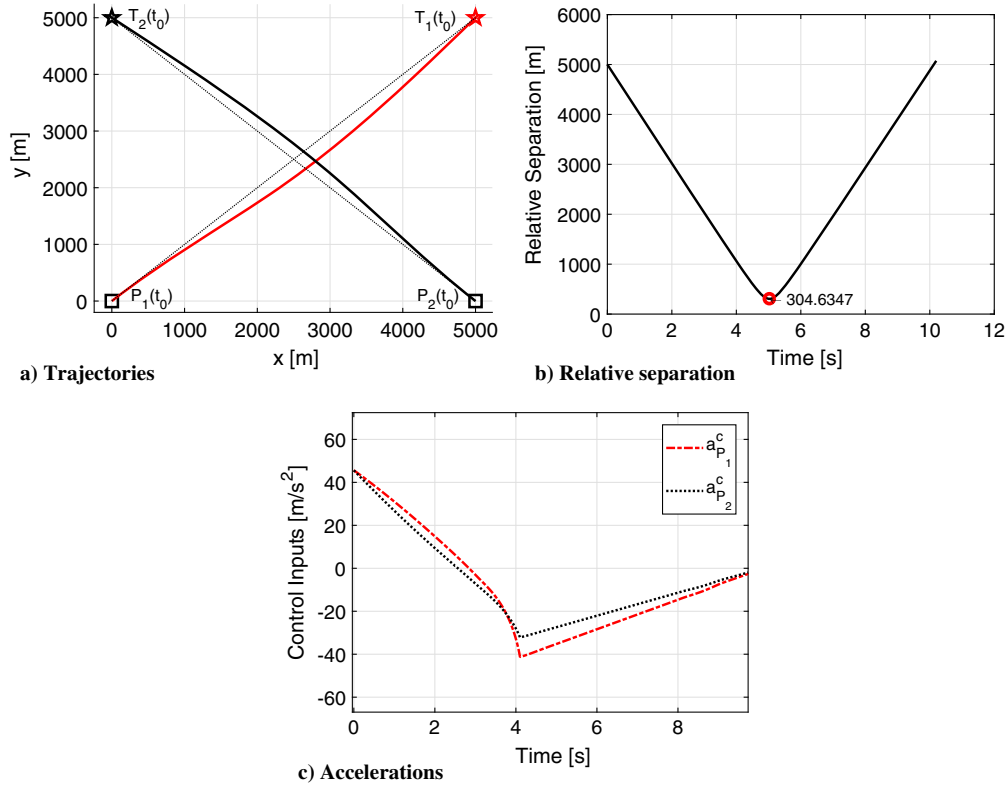


Fig. 4 Scenario 1: cooperative collision avoidance between identical pursuers ( $\alpha_1 = 1, \alpha_2 = 1$ ).

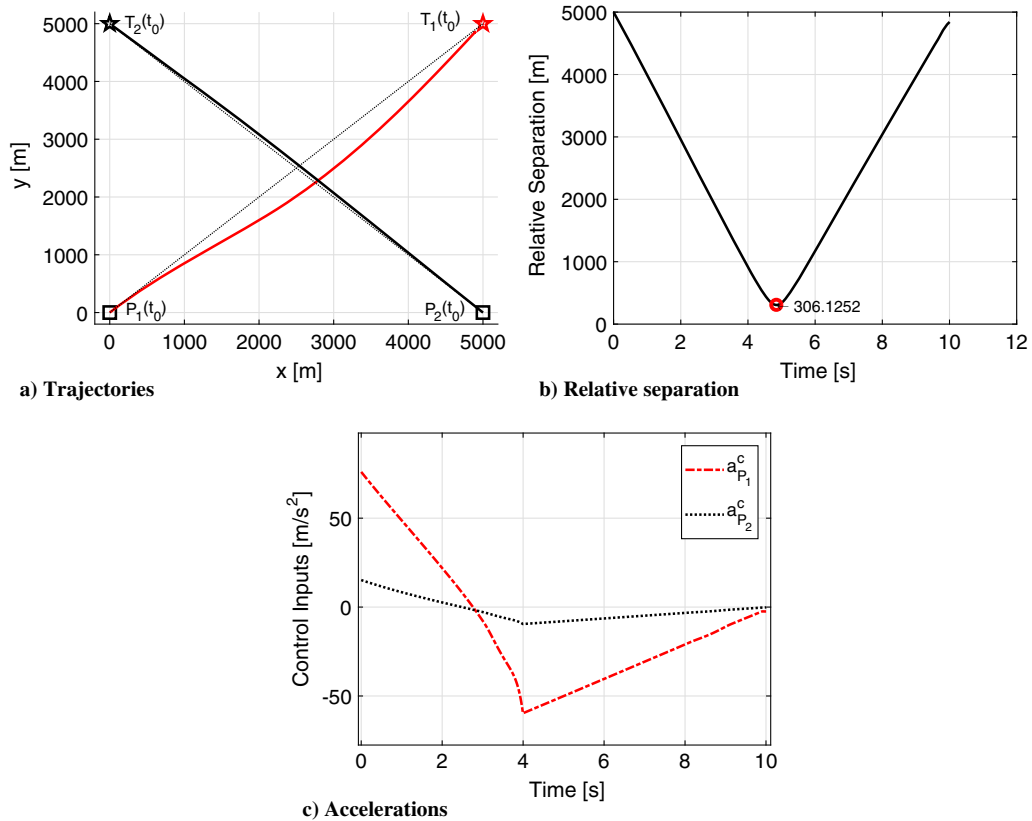


Fig. 5 Scenario 1: cooperative collision avoidance when pursuers have different maneuvering capabilities ( $\alpha_1 = 1, \alpha_2 = 10$ ).

platforms (see Fig. 8) with diameters of 0.35 m each were used as pursuers. The position information for each robot is obtained using Optitrack motion capture system, and their speed is estimated from the position data using a Savitzky–Golay digital filter [22]. The software platform used is an experimental framework developed at

CASY, which integrates Optitrack motion capture system and other robotic platforms with Simulink and Robot Operating System. The commands from the controller are computed off-board at an update rate of 30 Hz on a host computer and then sent to Kobuki base using 2.4 GHz standard WiFi protocol.

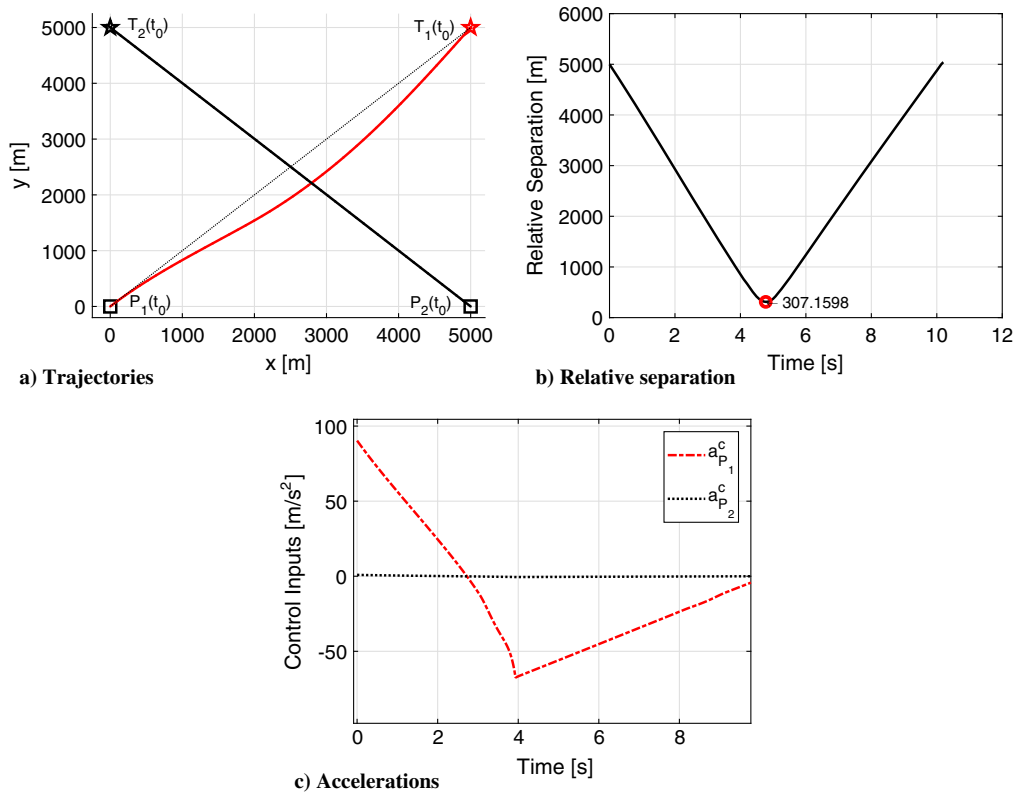


Fig. 6 Scenario 1: collision avoidance when one of the pursuers has severely limited maneuver capability ( $\alpha_1 = 1, \alpha_2 \rightarrow \infty$ ).

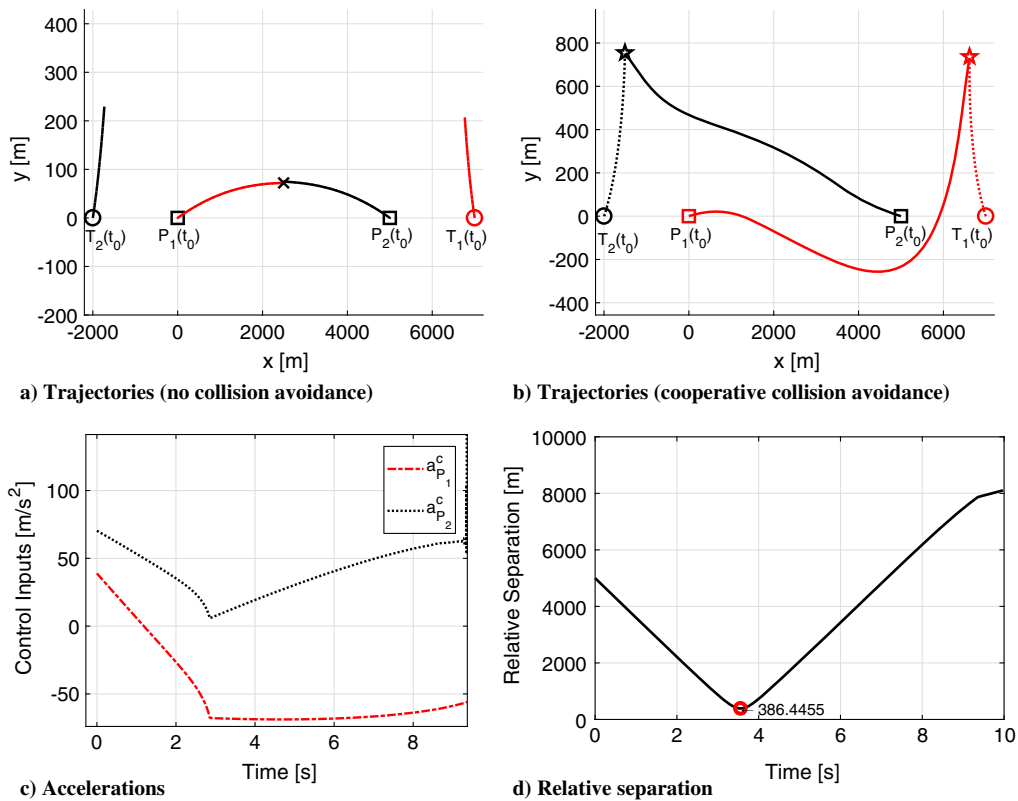


Fig. 7 Scenario 2: collision avoidance and interception of maneuvering targets ( $\alpha_1 = 1, \alpha_2 = 1$ ).

For all the experiments, the speeds of the robots were maintained constant using a linear-quadratic tracking controller described in [23]. The safe distance between the robots is measured between their geometrical centers and is considered to be 0.40 m. The parameters of the experiments are summarized in Table 2.

Figure 9 shows the results when both robots have similar maneuvering capabilities and cooperate with each other equally to avoid collision. Trajectories of both the robots are shown in Fig. 9a. The LOS joining the robots and their respective target points are shown in dotted lines. Similarly, for the case when one robot has



Fig. 8 Kobuki robotic platform.

Table 2 Parameters for experiment

Parameter	Value
Initial position of $P_1$ , m	(-1.8, -2.3)
Initial position of $P_2$ , m	(-1.8, 1.0)
Initial position of $T_1$ , m	(1.8, 1.0)
Initial position of $T_2$ , m	(1.8, -2.3)
Speed of pursuers ( $V_{P_1}, V_{P_2}$ ), m/s	(0.3, 0.3)
Speed of targets ( $V_{T_1}, V_{T_2}$ ), m/s	(0, 0)
Target accelerations ( $a_{T_1}^c, a_{T_2}^c$ ), m/s <sup>2</sup>	(0, 0)
Minimum safe distance $R$ , m	0.4

limited maneuvering capability, the trajectories and relative separation between the robots are shown in Figs. 10a and 10b, respectively. For both the preceding described cases, the nature of the

trajectories, although not identical, is similar to the one shown in simulations in Figs. 4a and 6a. In all cases, the robots successfully reach their target points, and from Figs. 9b and 10b, it can be seen that they maintain the minimum separation greater than 0.4 m at the time of closest approach. It is suggested to follow a conservative approach while choosing the value for the minimum separation because the delays in the system and nonideal dynamics of the robots might drive the robots closer than the safe limit.

By running various numerical and experimental validations, it was found that, as expected, the performance of the guidance law in nonlinear engagement scenarios is consistent whenever the near collision course approximations hold. In cases where the paths of the pursuers deviate significantly from the collision course, the estimations of time-to-go measurements in Eq. (54) are no more accurate. This leads to the degradation in the performance of the guidance law. Also, the nonideal dynamics of the pursuer and assumption of perfectly constant speed are attributed to the differences seen between the trajectories obtained in simulations and experimental validation.

### VII. Conclusions

In this paper, a cooperative guidance law for  $n$  pursuers, which integrates collision avoidance between the pursuers and ensures capture of their respective targets, was proposed. An optimal-control-based formulation was used to minimize the total team effort with different penalties on the control effort of each pursuer, while incorporating target interception and collision avoidance as state constraints. Using this formulation, the guidance laws for the pursuers were derived using the linearized engagement model and linear quadratic optimal control theory. For constantly maneuvering targets, the guidance law for each pursuer has the form of augmented proportional navigation, with additional terms corresponding to collision avoidance. A special case of two pursuers was considered, and an analytical solution of the guidance law for this case was obtained. In cases where one of the pursuers has a severely limited acceleration capabilities, the proposed guidance law amounts to performing the avoidance maneuver only by the other pursuer,

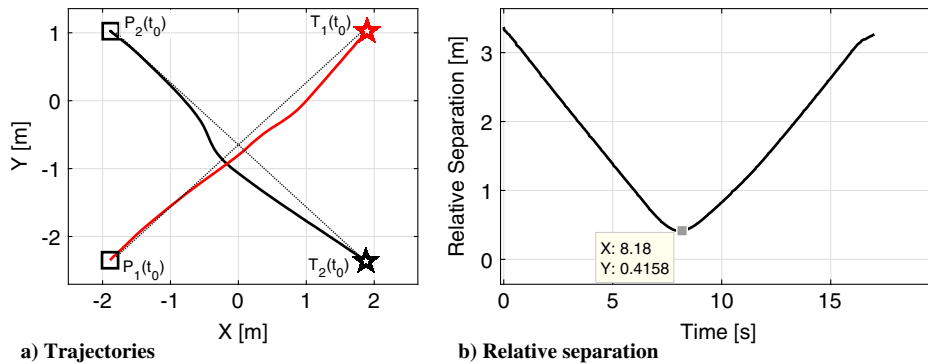


Fig. 9 Cooperative collision avoidance when both robots have similar maneuvering capabilities ( $\alpha_1 = 1, \alpha_2 = 1$ ).

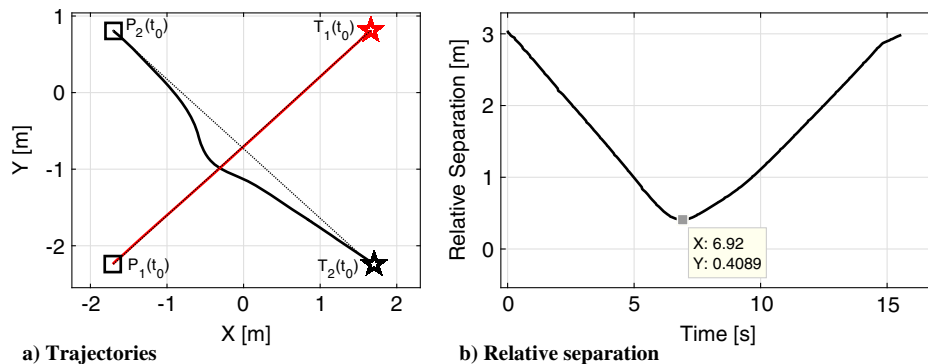


Fig. 10 Collision avoidance when one robot has severely limited maneuvering capability ( $\alpha_1 = 1000, \alpha_2 = 1$ ).

whereas the second pursuer performs only the intercept according to augmented proportional navigation guidance law. Simulations for both linear and nonlinear engagements and highlight the cooperation between the pursuers. The experimental validation also confirms the applicability of the guidance law, at least in the tested small indoor environments. The proposed guidance law requires estimates of the time-to-go between the different entities in the engagement scenario. A poor estimate of time-to-go in highly nonlinear scenarios will result in performance degradation.

### Appendix: Generalized Dead-Zone Function

The generalized dead-zone function  $\Psi_{S,Q}(\cdot): \mathbb{R}^N \rightarrow \mathbb{R}^N$  is proposed in [15,20]. It is associated with subset  $S \in \mathbb{R}^N$  and a positive-definite matrix  $Q \in \mathbb{R}^{N \times N}$ , such that

$$\Psi_{S,Q}(z) = Q(z^{d*} - z) \quad (\text{A1})$$

The minimizer  $z^{d*}$  is given by

$$z^{d*} = \arg \min_{z^d \in S} (z^d - z)^T Q (z^d - z) \quad (\text{A2})$$

Because  $Q$  is positive-definite, the minimum value  $z^{d*}$  always exists. In cases in which the set  $S$  is convex, the minimum value is unique, and the dead-zone function is unequivocally defined at each point. But this is not the case in our problem. Here,  $S$  is not even connected, and hence multiple solutions may exist. Fortunately, this occurs on a set of measure zero. Even more importantly, even in those cases in which the dead-zone function takes multiple values, each of them can be used for our purpose because each of these values corresponds to the optimum solution to the guidance problem.

### Acknowledgment

The research was supported by the A. Pazy Research Foundation.

### References

- [1] Fiorini, P., and Shiller, Z., "Motion Planning in Dynamic Environments Using Velocity Obstacles," *International Journal of Robotics Research*, Vol. 17, No. 7, 1998, pp. 760–772. doi:10.1177/027836499801700706
- [2] Chakravarthy, A., and Ghose, D., "Obstacle Avoidance in a Dynamic Environment: A Collision Cone Approach," *IEEE Transactions on Systems, Man, and Cybernetics—Part A: Systems and Humans*, Vol. 28, No. 5, 1998, pp. 562–574. doi:10.1109/3468.709600
- [3] Han, S.-C., Bang, H., and Yoo, C.-S., "Proportional Navigation-Based Collision Avoidance for UAVs," *International Journal of Control, Automation and Systems*, Vol. 7, No. 4, 2009, pp. 553–565. doi:10.1007/s12555-009-0407-1
- [4] Tony, L. A., Ghose, D., and Chakravarthy, A., "Precision UAV Collision Avoidance Using Computationally Efficient Avoidance Maps," *2018 AIAA Guidance, Navigation, and Control Conference*, AIAA Paper2018-0875, 2018. doi:10.2514/6.2018-0875
- [5] Khatib, O., "Real-Time Obstacle Avoidance for Manipulators and Mobile Robots," *International Journal of Robotics Research*, Vol. 5, No. 1, 1986, pp. 90–98. doi:10.1177/027836498600500106
- [6] Rimón, E., and Koditschek, D. E., "Exact Robot Navigation Using Artificial Potential Functions," *IEEE Transactions on Robotics and Automation*, Vol. 8, No. 5, 1992, pp. 501–518. doi:10.1109/70.163777
- [7] Ge, S. S., and Cui, Y. J., "New Potential Functions for Mobile Robot Path Planning," *IEEE Transactions on Robotics and Automation*, Vol. 16, No. 5, 2000, pp. 615–620. doi:10.1109/70.880813
- [8] Snape, J., Van den Berg, J., Guy, S. J., and Manocha, D., "The Hybrid Reciprocal Velocity Obstacle," *IEEE Transactions on Robotics*, Vol. 27, No. 4, 2011, pp. 696–706. doi:10.1109/TRO.2011.2120810
- [9] Sunkara, V. R., and Chakravarthy, A., "Cooperative Collision Avoidance and Formation Control for Objects with Heterogeneous Shapes," *IFAC—PapersOnLine*, Vol. 50, No. 1, 2017, pp. 10128–10135. doi:10.1016/j.ifacol.2017.08.1793
- [10] Zapoteczny-Anderson, P. M., and Ford, J. J., "Optimal-Stopping Control for Airborne Collision Avoidance and Return-to-Course Flight," *Australian Control Conference*, IEEE Publ., Piscataway, NJ, 2011, pp. 155–160.
- [11] Menon, P. K., and Park, S. G., "Dynamics and Control Technologies in Air Traffic Management," *Annual Reviews in Control*, Vol. 42, 2016, pp. 271–284. doi:10.1016/j.arcontrol.2016.09.012
- [12] Menon, P. K., Sweriduk, G. D., and Sridhar, B., "Optimal Strategies for Free-Flight Air Traffic Conflict Resolution," *Journal of Guidance, Control, and Dynamics*, Vol. 22, No. 2, 1999, pp. 202–211. doi:10.2514/2.4384
- [13] Škrjanc, I., and Klančar, G., "Optimal Cooperative Collision Avoidance Between Multiple Robots Based on Bernstein–Bézier Curves," *Robotics and Autonomous Systems*, Vol. 58, No. 1, 2010, pp. 1–9. doi:10.1016/j.robot.2009.09.003
- [14] Weiss, M., and Shima, T., "Linear Quadratic Optimal Control Based Missile Guidance Law with Obstacle Avoidance," *IEEE Transactions on Aerospace and Electronic Systems*, Vol. 99, No. 1, 2018, pp. 1–1. doi:10.1109/TAES.2018.2849901
- [15] Kumar, S. R., Weiss, M., and Shima, T., "Minimum-Effort Intercept Angle Guidance with Multiple-Obstacle Avoidance," *Journal of Guidance, Control, and Dynamics*, Vol. 41, No. 6, 2018, pp. 1355–1369. doi:10.2514/1.G003223
- [16] Bryson, A. E., *Applied Optimal Control: Optimization, Estimation and Control*, Routledge, New York, 1975, Chaps. 3, 5. doi:10.1201/9781315137667
- [17] Gutman, S., *Applied Min-Max Approach to Missile Guidance and Control*, AIAA, Reston, VA, 2005, pp. 232–236. doi:10.2514/4.476952
- [18] Ben-Asher, J., and Yaesh, I., *Advances in Missile Guidance Theory*, Vol. 180, Progress in Astronautics and Aeronautics, AIAA, Reston, VA, 1998, Chap. 7.
- [19] Horn, R. A., Horn, R. A., and Johnson, C. R., *Matrix Analysis*, Cambridge Univ. Press, New York, 1990.
- [20] Weiss, M., Shima, T., Castaneda, D., and Rusnak, I., "Combined and Cooperative Minimum-Effort Guidance Algorithms in an Active Aircraft Defense Scenario," *Journal of Guidance, Control, and Dynamics*, Vol. 40, No. 5, 2017, pp. 1241–1254. doi:10.2514/1.G002315
- [21] Jha, B., Turetsky, V., and Shima, T., "Robust Path Tracking by a Dubins Ground Vehicle," *IEEE Transactions on Control Systems Technology*, 2018. doi:10.1109/TCST.2018.2870571
- [22] Schafer, R. W., "What Is a Savitzky–Golay Filter?" *IEEE Signal Processing Magazine*, Vol. 28, No. 4, 2011, pp. 111–117. doi:10.1109/MSP.2011.941097
- [23] Jha, B., Turetsky, V., and Shima, T., "Linear-Quadratic Robust Path Tracking for a Dubins Vehicle," *2018 European Control Conference*, IEEE Publ., Piscataway, NJ, 2018, pp. 2101–2106. doi:10.23919/ecc.2018.8550513